PEM Fuel Cell Drying and Flooding Diagnosis With Signals Injected by a Power Converter

Giovanni Dotelli, Roberto Ferrero, *Member, IEEE*, Paola Gallo Stampino, Saverio Latorrata, and Sergio Toscani, *Member, IEEE*

I. Introduction

COST and reliability are two key aspects that still hinder a massive-scale market diffusion of fuel cell (FC) technology. For this reason, the development of low-cost diagnostic tools and control systems able to guarantee a reliable long-term FC operation appears as a primary objective to be pursued in the next years.

In particular, for polymer electrolyte membrane (PEM) FCs, a continuous monitoring of the cell water content would be extremely important, as it deeply affects the FC efficiency, voltage stability, and lifetime. Indeed, an excessively low water content in the FC membrane causes an increase in ohmic losses and possible membrane damage, while too much water can lead to flooding of the gas channels, and of the porous catalyst and gas diffusion layers, which in turn causes again a reduction in power output [1], [2]. Electrochemical impedance spectroscopy is well known to be a powerful technique to identify performance degradation induced by different phenomena, among which membrane drying and cell flooding [3]–[7], but its typical use in laboratory tests envisages dedicated instrumentation, whose cost and complexity make it not suitable for low-cost commercial applications.

As a partial solution for this problem, for what concerns the dehydration diagnosis, a few works [8]–[10] suggested the use of the current ripple produced by switch-mode power converters to measure the FC equivalent ohmic resistance, which is a good indicator for the membrane water content. Indeed, the converter switching acts as a perturbation allowing one to acquire the FC frequency response at the ripple frequencies, which are typically in the kilohertz range where the cell impedance practically reduces to the ohmic resistance.

In [11], we tested this diagnostic approach with a dc/dc boost converter connected to a single PEM FC, showing that quite accurate measurements of the ohmic resistance can be obtained if suitable model-based elaboration algorithms are employed, considering the nonsinusoidal nature of the ripple and the reactive behavior of the FC.

Starting from this result, this paper aims at showing how an *ad hoc* switching control of the converter allows introducing low-frequency components in the ripple waveform that can be used to estimate the FC low-frequency impedance, suitable for flooding diagnosis, so that both opposite failure modes associated with water management can be detected from the converter ripple alone. Similar techniques have been already successfully employed in different applications, such as fault detection in electrical machines [12]–[14], but to the best of the authors' knowledge, its application to FCs for flooding diagnosis has not been investigated yet.

Low-frequency measurements on PEM FCs present particular challenges that need to be addressed for a reliable diagnosis, which is also discussed in this paper. First, the complex electrochemical processes occurring within the cell give rise to continuous oscillations in the output voltage, preventing from obtaining accurate low-frequency impedance measurements, particularly in flooded conditions. Second, different FC operation modes (e.g., constant current, constant voltage, or constant power) produce different responses to performance degradations due to drying or flooding, which may affect the sensitivity required to the diagnostic algorithm to correctly recognize these two failure modes. To deal with these issues, suitable measurement techniques and diagnostic algorithms need to be developed.

Manuscript received November 10, 2014; revised January 7, 2015; accepted February 6, 2015. Date of publication March 19, 2015; date of current version July 10, 2015. The Associate Editor coordinating the review process was Dr. Carlo Muscas.

G. Dotelli, P. G. Stampino, and S. Latorrata are with the Department of Chemistry, Materials, and Chemical Engineering G. Natta, Politecnico di Milano, Milan 20133, Italy (e-mail: giovanni.dotelli@polimi.it; paola.gallo@polimi.it; saverio.latorrata@polimi.it).

R. Ferrero is with the Department of Electrical Engineering and Electronics, University of Liverpool, Liverpool L69 3BX, U.K. (e-mail: roberto.ferrero@liverpool.ac.uk).

S. Toscani is with the Dipartimento di Elettronica, Informazione e Bioingegneria, Politecnico di Milano, Milan 20133, Italy (e-mail: sergio.toscani@polimi.it).

Color versions of one or more of the figures in this paper are available online.

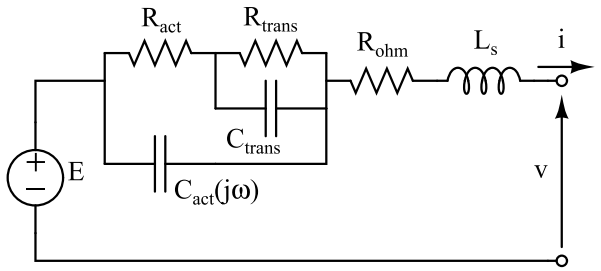

Fig. 1. Typical linearized equivalent circuit of a PEM FC.

II. FC Drying and Flooding

The three main causes of voltage drop in a PEM FC are associated with ohmic losses, activation polarization, and mass transport limitation, respectively. Although these phenomena are generally described by nonlinear models, the simple linear equivalent circuit shown in Fig. 1 is often adequate to describe the FC behavior around a stable operating point. The three equivalent resistances are associated with the three causes of voltage drop mentioned above, while the two equivalent capacitances describe the dynamic response of activation and transport phenomena. A frequency-dependent capacitance $C_{\text{act}}(j\omega)$ [15] or a constant-phase element instead of it [6] is usually required for a better fit of the actual FC response. Finally, a series inductance has been added to consider inductive phenomena that are likely to appear at high frequencies, mainly due to the FC electrical connections. It is worth noting that all the equivalent electrical parameters associated with activation and transport processes are strongly dependent on the FC working point, as better explained in the following sections.

As far as water management is concerned, membrane dehydration produces a decrease of the membrane ionic conductivity and therefore an increase of the equivalent ohmic resistance R_{ohm}, while cell flooding due to water accumulation in the gas channels and/or in the gas diffusion layer hinders the gas transport, and therefore, it produces an increase of the equivalent transport resistance R_{trans}, as well as of the equivalent capacitance C_{trans}. For this reason, a combined monitoring of the ohmic resistance and the low-frequency impedance (sensitive to the transport resistance), by acquiring either the whole spectrum [4]–[6] or single-frequency impedances [7], is generally considered as an effective approach to detect both drying and flooding occurrences and to distinguish between them.

While it is known that ohmic resistance measurements can be inexpensively obtained by exploiting the high-frequency ripple of switch-mode converters, as mentioned in the previous section, lower-frequency measurements are usually performed by dedicated and more sophisticated instrumentation, such as frequency response analyzers, that cannot be afforded in commercial applications. The high complexity and cost of such instrumentation arise not only from the need to generate perturbation signals over a wide range of frequencies but also from the requirement of accurate measurements with low-amplitude signals because of the nonlinear FC response appearing at low frequencies.

Alternative solutions for flooding diagnosis involving nonelectrical quantities have been studied to overcome this problem, among which the simplest one from the implementation point of view is based on gas pressure drop measurements between inlet and outlet gas channels [16], [17]. However, although pressure measurements are very useful to detect flooding in its first stage, the relationship between pressure drop and FC electrical performance is not straightforward [18]. Thus, the impedance should be always measured in addition to pressure for a more reliable diagnosis.

The following sections will explain how both low-frequency and high-frequency impedance measurements with satisfying accuracy can be performed by exploiting the ripple produced by a switch-mode power converter connected to the FC, without need of additional expensive instrumentation.

III. Injection of Low and High Frequency Components

Switch-mode converters are usually employed to connect FCs to their loads or to integrate them with other energy sources in hybrid power systems. Since the applications are extremely heterogeneous, a great variety of power electronics architectures can be found in both industrial products and literature (see [19]).

The power electronic converters have to be controlled to ensure proper FC operation and, of course, deliver the required power to the load. In stand-alone applications [20], [21], neglecting the losses, FC power output should match the load power. Since FC time constants are fairly slow, in the presence of fast perturbations, the power converter should adjust the operating point on the V–I curve to ensure power balance. This architecture cannot be employed when the load profile contains large and fast power variations. In this case, an hybrid FC system is generally employed: other power sources or energy storage systems are introduced, so that the dynamic characteristics are greatly improved, the peak power output is also enhanced while the FC operates in almost stationary conditions. In general, the switch-mode power converter connected to the FC controls its current [22]. However, in some architectures, known as direct parallel structures, the auxiliary power sources and the load are interfaced to a dc bus by means of proper power converters, while the FC is directly connected to the dc bus [23]. Since the dc bus voltage is controlled, in this case, the FC operates at constant voltage.

The voltage or current controller can be employed to introduce low-frequency perturbations in the FC current or voltage waveforms, respectively, superimposed onto the dc reference values. If properly chosen, such perturbations permit to monitor the low-frequency impedance of the FC, which can be used to detect flooding occurrence. Of course, these additional perturbations increase power losses, and thus, it is necessary to keep their amplitudes as low as possible, also because the FC low-frequency response is not linear, and therefore, impedance measurements require low-amplitude signals.

It is well known that when power electronic converters are employed, currents and voltages include high-frequency ripple; assuming constant switching frequency operation, such

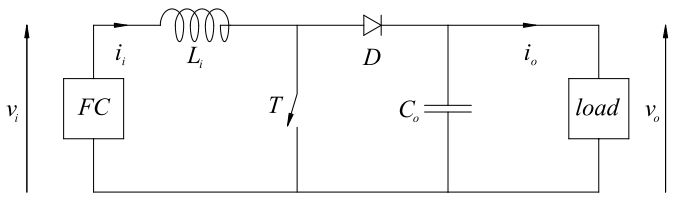

Fig. 2. Schematic of a dc/dc boost converter connected to the FC on one side and to an electrical load on the other side.

as in pulse width modulation (PWM) controlled converters, the frequencies of these components are approximately multiples of the switching frequency. Having chosen a typical switching frequency of some kilohertz, the ripple inherently produced by the converter is also contained in the FC current and voltage, superimposed onto their dc values. Therefore, it can be exploited to measure the high-frequency part of the cell impedance spectrum. Considering the equivalent circuit of Fig. 1, the transport dynamics as well as the frequency dependence of the activation capacitance $C_{\text{act}}(j\omega)$ can be neglected, so that either a first-order RC or RL circuit adequately describes the FC response at the main ripple frequencies, depending on the converter switching frequency and on the cutoff frequencies of the equivalent circuit. In both cases, fitting the available impedance data with the proper first-order model provides accurate estimates of the ohmic resistance R_{ohm} that can be used for membrane drying diagnosis [11], as shown in Section VII.

IV. Design of the FC Converter

To test the proposed diagnostic method based on the injection of low- and high-frequency components, a case study has been chosen. In particular, the FC is connected to the load by means of a PWM-controlled boost dc/dc converter. Besides its simplicity, it is frequently employed in FC applications, and its architecture is shown in Fig. 2.

Let us introduce the duty cycle δ as the fraction of the switching period when the switch T is turned on. Assuming that the duty cycle changes slowly, the power converter introduces spectral components in the cell current and voltage whose frequencies are multiples of the switching frequency f_{sw}. When considering the continuous conduction mode and neglecting the losses, the relationship between the input and output voltages (V_i and V_o, respectively) is given by

$$V_o = \frac{V_i}{1-\delta}. \tag{1}$$

The choice of the reactive components (input inductor and output capacitor) depends on the FC working point (input current and voltage), the desired ripple amplitudes of the input current (ΔI_i) and output voltage (ΔV_o), respectively, and the converter switching frequency f_{sw} and duty cycle δ. In particular, the peak-to-peak amplitude of the input current ripple is given by the well-known formula for the boost converter

$$\Delta I_i = \frac{V_i}{f_{\text{sw}} L_i}\delta \tag{2}$$

while the peak-to-peak amplitude of the output voltage can be computed as

$$\Delta V_o = \frac{(1-\delta)\delta}{C_o f_{\text{sw}}} I_i \tag{3}$$

assuming that the entire ripple in the output current flows through the capacitor.

Limiting the amplitude of the current ripple is vital for FC applications. Several papers [15], [24]–[27] have investigated the negative effects that current ripple might produce on a FC, such as loss increase, possible damages, and durability decrease, but a complete understanding of all these phenomena has not been achieved yet, and therefore, a generally-accepted indication of the maximum allowed ripple is presently not available. Nevertheless, a reasonable ripple amplitude that can be considered to have a negligible effect on both the FC operation and lifetime is 5% peak-to-peak of the rated current.

With these assumptions, considering the 20-A rated current of the cell employed for the experimental tests (corresponding to a cell voltage of about 0.5 V in nominal conditions) and a switching frequency of 10 kHz, the input inductance results in the value $L_i = 50\ \mu$H, in the most conservative condition that occurs for $\delta = 1$. On the other hand, accepting a peak-to-peak ripple not greater than 0.1 V in the output voltage, the required output capacitance C_o is found to be 5 mF calculated in the most conservative condition, now $\delta = 0.5$.

V. Switching Control Strategy

As previously explained in Section III, switch-mode converters can be controlled so as to inject a low-frequency perturbation in the FC current or voltage. This perturbation signal can be properly designed to allow an effective flooding detection. It is known that flooding affects the transport dynamics and therefore it causes an increase of the equivalent transport resistance R_{trans}. The highest sensitivity of the FC impedance with respect to this parameter is achieved at the limit low frequency of the impedance spectrum, where the impedance equals the sum of all resistances ($R_{\text{ohm}} + R_{\text{act}} + R_{\text{trans}}$). Unfortunately, this limit frequency is quite low, typically below 1 Hz, and in flooded conditions, it becomes even lower because of the increase of both R_{trans} and C_{trans}. Thus, a frequency lower than 100 mHz would be required for this measurement, while it is known that it is practically impossible to perform accurate measurements at such frequencies, particularly in flooded conditions, because of instabilities in the FC internal state.

As a possible solution, multiple impedance measurements at higher frequencies are suggested instead of a single low-frequency measurement. The limit impedance value at low frequency would be then calculated by fitting the available measurements with a first-order RC model. In this case, reasonably accurate measurements can be performed even in flooded conditions. Therefore, a multisine signal having a 0.5-Hz fundamental frequency, containing the harmonics of order 2, 3, 5, and 8, has been chosen as voltage or current perturbation; the spacing of the frequency components is quasi-logarithmic, and all of them have the same magnitude.

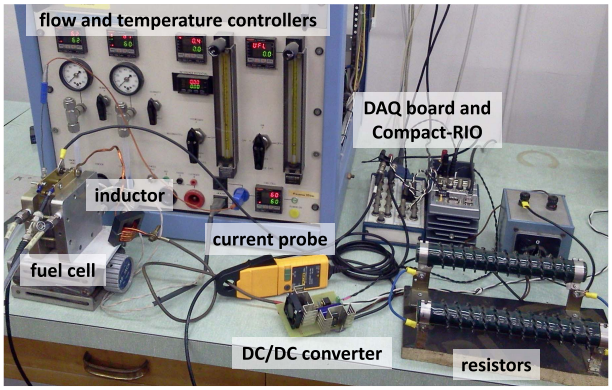

Fig. 3. Photograph of the experimental setup.

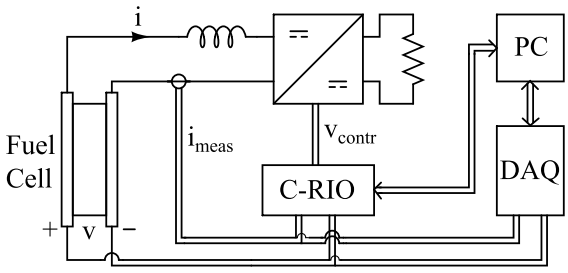

Fig. 4. Block diagram of the experimental setup.

The behavior of the FC may become nonlinear if the amplitude of the perturbation is excessive; furthermore, large perturbations may also jeopardize the life expectancy of the FC. For this reason, the phases of the harmonics in the signal have been optimized to minimize the peak-to-rms ratio, often known as crest factor. In this way, the power of the signal (and therefore the accuracy of the measurements) is enhanced for a given peak-to-peak amplitude of the perturbation. A 0.2-A peak-to-peak amplitude of the current oscillation was chosen, so that it is about 40% of the high-frequency ripple amplitude. The corresponding amplitude of the voltage oscillation in controlled voltage operation was then calculated based on the expected low-frequency impedance in nominal conditions.

The boost converter can impose either the FC voltage or current. A simple integral controller is employed, and it has been tuned so that the cutoff frequency of the loop is 400 Hz when operating with a duty cycle of 0.7. Therefore, the waveforms of both the current and voltage perturbations can be accurately applied to the FC.

VI. Experimental Setup

The FC employed for the experimental tests is a single PEM cell composed of commercial materials, in particular, a Nafion 212 membrane as electrolyte (23-cm^2 active area and 50-μm thickness) and a gas diffusion electrode reference sample (E-TEK LT140). The cell is fed with pure hydrogen and air at the anode and cathode, respectively, whose flow rates are measured and controlled by calibrated flow meters. Both inlet gases are humidified through saturators, whose temperatures are controlled to achieve the desired relative humidity. Finally, the cell temperature is kept constant at 60 °C.

A photograph and a block diagram of the whole experimental setup are shown in Figs. 3 and 4, respectively. The cell is directly connected to the dc/dc converter, whose output is in turn connected to a resistive load. The inductor visible in Fig. 3 is the 50-μH input inductance designed for a 10-kHz switching frequency, while if the converter is operated with a lower switching frequency, a larger inductance value is required to maintain the input current ripple within the design specifications. The control of the electronic switch, according to the strategy described in the previous section, is provided by a reconfigurable input/output system (National Instrument Compact-RIO 9014), where the control algorithm is implemented in the internal Xilinx Virtex-II 3-million-gate FPGA to guarantee real-time operation. The cell current measurement is provided by a Hall effect current probe with a 100-kHz bandwidth (Fluke i30s), whose voltage output is acquired by the Compact-RIO 16-bit analog input module (NI 9215) together with the cell voltage, with 10^5 samples-per-second sampling frequency (a four-terminal measurement is performed to avoid the effects of contact resistances). These two signals are also acquired by a 16-bit data acquisition (DAQ) system (NI 6251) synchronized with the Compact-RIO, with a higher sampling frequency ($2.5 \cdot 10^5$ samples-per-second), more suitable for the signal processing required for diagnostics.

It is worth noting that for the implementation in a commercial application, most of the above-mentioned hardware would be replaced by the devices already present in the original application design, including the dc/dc converter, its controller, and in some cases also a suitable current transducer and a DAQ system, thus dramatically reducing the implementation costs of the proposed technique. Even when a current transducer, a DAQ system, and a proper processing unit have to be specifically added, the cost of this system is likely to be at least one order of magnitude lower than laboratory impedance measurement systems based on frequency response analyzers.

VII. Impedance Measurements

The first tests in stationary conditions were carried out to illustrate the proposed procedure to estimate the FC ohmic resistance and low-frequency limit resistance from the high- and low-frequency ripple components, respectively, by means of proper fitting of the available impedance data at different frequencies. For these tests, the cell was operated at a medium-level dc of 13 A, with fully humidified inlet gases and nominal flow rates (0.2 Nl/min for hydrogen and 1.0 Nl/min for air). The load was adjusted to make the converter operate with a duty cycle around 0.7.

A. Ohmic Resistance

The procedure for ohmic resistance identification was tested with two different switching frequencies, namely, 1 and 10 kHz, properly chosen for the cell under test to show the capacitive and inductive responses, respectively. Although 1 kHz is lower than typically employed switching frequencies, this choice allows to illustrate how two different models can be used to equally well estimate the ohmic resistance in different cases, considering that for a different FC, the frequencies at

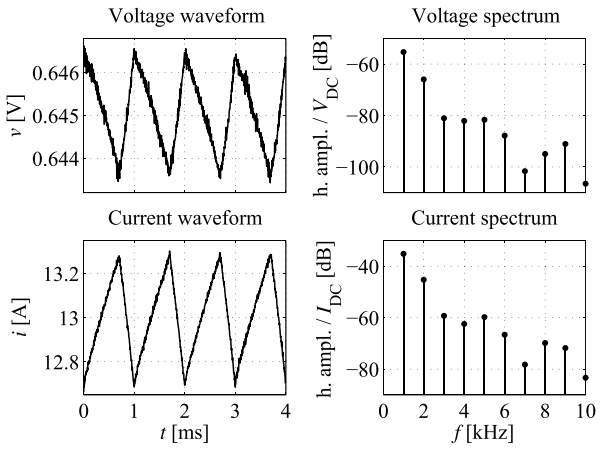

Fig. 5. Measured high-frequency FC voltage and current ripple and their Fourier spectra, obtained with a 1-kHz switching frequency and a 0.7 duty cycle.

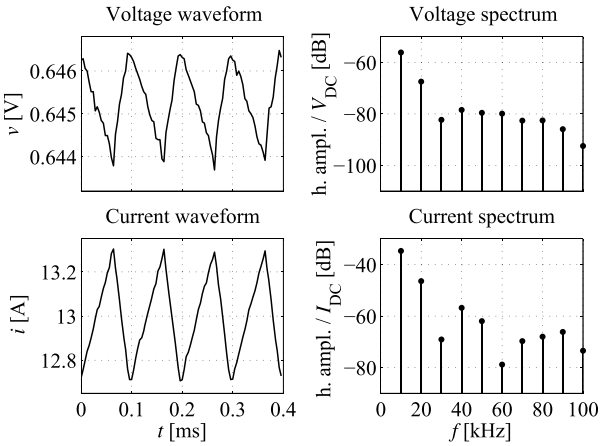

Fig. 6. Measured high-frequency FC voltage and current ripple and their Fourier spectra, obtained with a 10-kHz switching frequency and a 0.7 duty cycle.

which the capacitive and inductive responses are seen may be slightly different.

The measured cell voltage and current waveforms with the two switching frequencies are reported in Figs. 5 and 6, respectively, together with their Fourier spectra. For the impedance evaluation in both tests, the voltage and current spectra were calculated on a time window corresponding to 50 switching periods and averaged over a time window of 1 s, where the cell impedance is not expected to significantly change. The impedance spectrum was then calculated as complex ratio between these voltage and current spectra. While the mean value of the measurements provides the best estimate of the cell impedance, their standard deviation provides an estimate of the associated uncertainty mainly due to uncontrollable variations of the FC internal conditions that can be used for a weighted least-squares fitting. This so-called type-A uncertainty is typically greater than the type-B uncertainty contribution arising from the instrumentation accuracy, and therefore, it should be regarded as the best uncertainty estimate, particularly, when it has to be employed to correctly recognize impedance variations due to faults, as in this application.

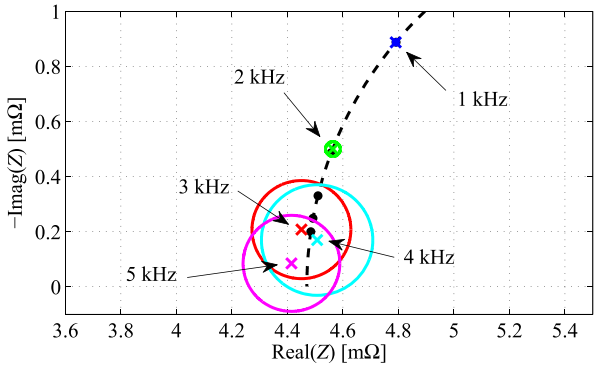

Fig. 7. High-frequency impedance measurements (crosses) and their standard deviations (circles) in a 1-s time interval, obtained with a 1-kHz switching frequency, compared with the best fit according to (4) (dashed line and dots).

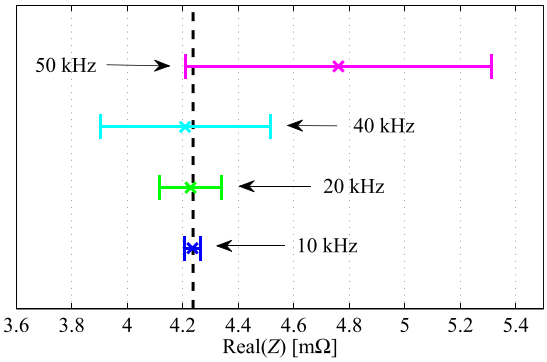

Fig. 8. Real parts of the high-frequency impedance measurements (crosses) and their standard deviations (bars) in a 1-s time interval, obtained with a 10-kHz switching frequency, compared with the best estimate of R_{ohm} (dashed line).

As far as the operation with a 1-kHz switching frequency is concerned, the impedances associated with the first five harmonic components (which are the most significant ones, according to Fig. 5), measured in a 1-s time interval, are shown in Fig. 7 (mean values and standard deviation circles) together with the best fit with a first-order RC model

$$Z(j\omega) = R_{\text{ohm}} + \frac{R_{\text{act}}}{1 + j\omega R_{\text{act}} C_{\text{act}}}. \tag{4}$$

The compatibility between model and experimental data at all considered frequencies confirms the model validity for the purposes of this paper, meaning that no significant definitional uncertainty is added to the uncertainty estimate of the equivalent ohmic resistance.

On the other hand, with a 10-kHz switching frequency, the cell response is better described by a first-order RL model

$$Z(j\omega) = R_{\text{ohm}} + j\omega L_s. \tag{5}$$

In this case, the ohmic resistance can be estimated considering only the real parts of the impedances shown in Fig. 8 for the most significant frequencies (those for this test are only the first, second, fourth and fifth harmonic components, as shown in Fig. 6). Again, the estimated ohmic resistance is compatible with the measurement results at all considered frequencies.

The slightly different values of R_{ohm} estimated in Figs. 7 and 8 can be explained by the above-mentioned

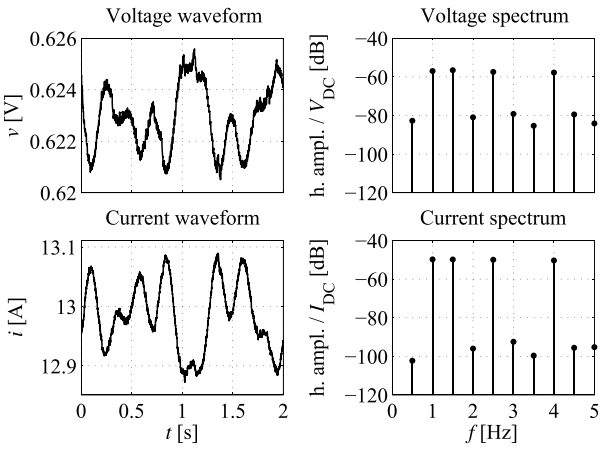

Fig. 9. Measured low-frequency FC voltage and current ripple introduced by the converter in current-control mode, and their Fourier spectra.

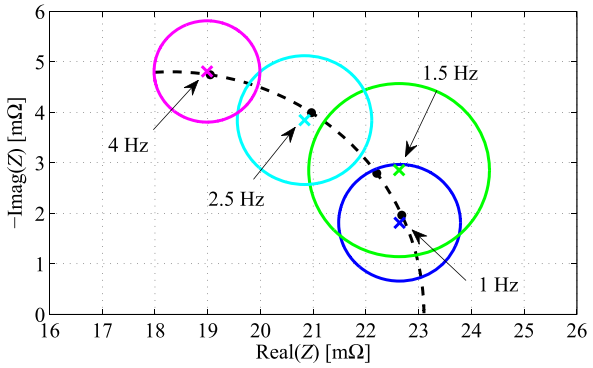

Fig. 10. Impedance measurements (crosses) and their standard deviations (circles) in a 20-s time interval, obtained from the low-frequency ripple, compared with the best fit according to (6) (dashed line and dots).

uncontrollable variations of the cell internal conditions [28] and they are in agreement with the type-A uncertainty estimated from repeated measurements, which is less than 0.2 mΩ in both cases. This uncertainty level defines the sensitivity of the proposed measurement method for drying diagnosis, as only ohmic resistance variations greater than this threshold can be considered as significant and thus associated with nonproper FC operation. This level is low enough to allow an effective detection of membrane dehydration in the cell under test, which is likely to produce R_{ohm} variations of 1 mΩ or more [10].

Finally, it should be noted that the cell temperature here is kept constant, while in some commercial applications, the FC stack is self-heated, without any temperature controller. When this occurs, the ohmic resistance may also vary as a consequence of temperature variations and this must be considered to correctly distinguish the resistance variations associated with the membrane humidification. Usually, if the cell temperature is measured, the effects of temperature can be compensated by assuming a linear relationship between temperature and membrane conductivity in the operating temperature range. As an example, for the cell under test, the increase in the ohmic conductance (i.e., the inverse of the ohmic resistance) with temperature is about 1.5 S/°C, with a nominal conductance value of about 200 S at 60 °C.

B. Low-Frequency Resistance

Similarly to what was done for the ohmic resistance, also the low-frequency limit resistance is estimated by fitting the four impedance measurements obtained by introducing low-frequency perturbations in the ripple waveform, as described in Section V. Again, a first-order *RC* model is employed for data fitting

$$Z(j\omega) = R_{\text{ohm}} + R_{\text{act}} + \frac{R_{\text{trans}}}{1 + j\omega R_{\text{trans}} C_{\text{trans}}}. \qquad (6)$$

The measured voltage and current waveforms in a one-period window, obtained with the converter operating in current-control mode, are reported in Fig. 9 together with their Fourier spectra, having filtered the high-frequency ripple. For the resistance identification, the spectra were averaged over a time window of 20 s to calculate their mean value and standard deviation. These values are reported in Fig. 10 together with the weighted least squares fit, showing also in this case the compatibility between the model and experimental data. The same considerations for the uncertainty evaluation reported above apply also to the low-frequency resistance, whose uncertainty is estimated to be about 1 mΩ in these experimental conditions, while the expected resistance variations in the case of flooding are one order of magnitude higher.

VIII. Fault Detection

As already explained, the high- and low-frequency resistance measurements described above are intended to be used to detect FC performance degradation due to membrane drying or cell flooding. The use of the ohmic resistance measurement for drying diagnosis has been already widely discussed in the literature, and results obtained on the cell under test were already presented in [10]. On the other hand, low-frequency measurements for flooding diagnosis require a deeper discussion, because the low-frequency impedance not only depends on the cell water content but also on the working point (i.e., the cell dc). This means that the converter control strategy defining the FC operation mode (e.g., constant current, constant voltage, or constant power) affects the impedance variations seen as a consequence of flooding events, and this should be considered in the flooding diagnosis.

To better illustrate this phenomenon in reproducible experimental conditions, mass transport was hindered by decreasing the inlet gas flow rates instead of increasing the gas relative humidity. This procedure is commonly employed in literature (see [4], [5] and [7]) to emulate flooding transients, being the effect on the mass transport dynamics very similar, as in both cases, fuel and oxygen starvation arises. The advantage of this choice is that the experimental conditions are better controllable and results show a much higher reproducibility.

The cell polarization curves with nominal gas flow rates (0.20 and 1.00 Nl/min for hydrogen and air, respectively) and decreased flow rates (0.14 and 0.53 Nl/min), with 85% gas relative humidity, are reported in Fig. 11. As expected, the

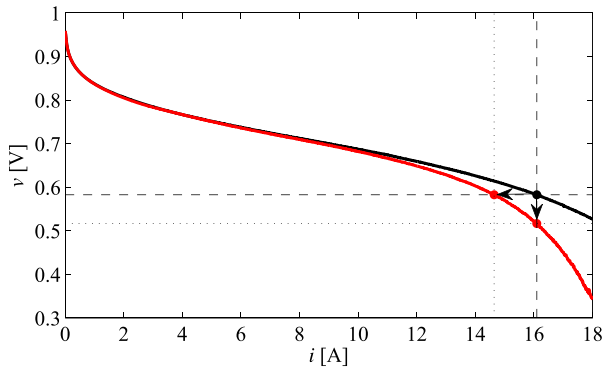

Fig. 11. FC polarization curves measured with nominal gas flow rates (upper black curve) and decreased flow rates (lower red curve), with 85% gas relative humidity; the selected working point ($I_{dc} = 16.1$ A) is shown with a black dot and the effects of constant-current and constant-voltage controls are illustrated.

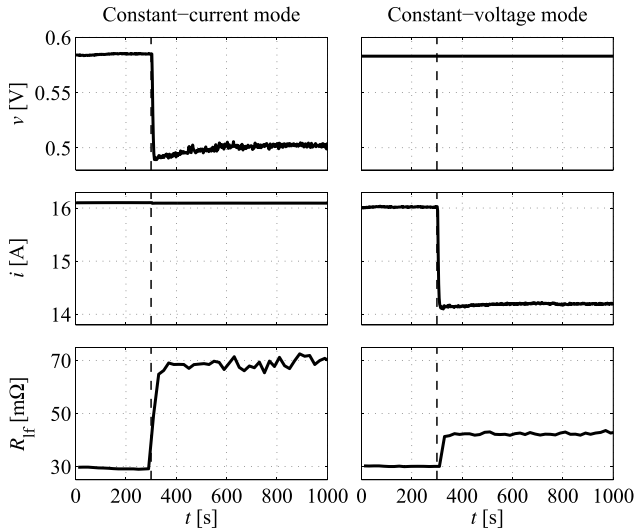

Fig. 12. Effects of a gas flow rate step variation from 0.20 and 1.00 Nl/min for hydrogen and air, respectively, to 0.14 and 0.53 Nl/min, in constant-current and constant-voltage operation modes; the cell voltage (top), current (middle), and low-frequency-limit resistance (bottom) are reported in the two cases.

lower flow rates limit the cell performances at high currents, where the fuel and oxygen consumption is higher. For the tests, a dc of 16.1 A was chosen corresponding to 0.7 A/cm^2. The effects of constant-current and constant-voltage controls when moving from the nominal curve to the lower curve are also shown in Fig. 11. Clearly, the former enhances the effects of gas starvation, while the latter has a stabilizing effect, making the cell work at lower current, where the difference between the two polarization curves is much smaller. If a constant-power control were implemented, its effect would be to make the cell operate at higher current, thus enhancing the effect of gas starvation even more. This is not shown in Fig. 11 because the maximum power of the lower curve is smaller than the power of the selected working point on the nominal curve.

The cell response to a step variation of the gas flow rates from the nominal ones (corresponding to the stoichiometric ratios $\lambda = 1.8$ and 3.7 at anode and cathode, respectively) to the decreased values (corresponding to $\lambda = 1.2$ and 2.0) is reported in Fig. 12, for the two cases of constant-current and constant-voltage operation modes. The flow rate variation is produced at $t = 300$ s, immediately followed by a voltage or current variation according to Fig. 11. The ohmic resistance does not show significant variations, and therefore, it is not reported in Fig. 12. On the contrary, the low-frequency resistance significantly increases as expected. It is worth noting that the resistance increase in constant-current mode is more than three times greater than in constant-voltage mode. This has two important implications from the flooding diagnosis point of view. First, the detection of impedance variations in constant-voltage mode requires a higher sensitivity. Second, the evaluation of the extent of flooding from impedance measurements needs to consider the operation mode chosen for the cell.

IX. Conclusion

A dc/dc boost converter for a single PEM FC was designed and built to test the possibility to use the current ripple produced by the converter for low-cost state-of-health diagnosis, suitable for commercial applications. In particular, the high-frequency ripple inherently produced by the converter allows one to measure the equivalent ohmic resistance, useful as an indicator for membrane dehydration, while the introduction of *ad hoc* low-frequency perturbations by properly acting on the switching control allows one to measure also the low-frequency impedance, suitable to detect cell flooding as well as other phenomena affecting the mass transport dynamics.

Accurate estimates of both the ohmic resistance and the low-frequency limit resistance were obtained using elaboration algorithms based on simple equivalent circuits that consider the nonsinusoidal nature of the ripple and the reactive behavior of the FC. The sensitivity required for low-frequency resistance measurements is discussed considering the effects of different control strategies of the converter defining different operation modes of the cell, such as constant-current and constant-voltage operations.

Experimental tests performed on a single cell confirmed the validity of the proposed approach and encourage further developments toward its application to commercial devices, involving stacks of several cells connected in series. In this case, depending on the stack size and on the available DAQ system, the voltages of single cells or small groups of cells can be acquired using a multiplexed architecture (thus without significantly increasing the acquisition system complexity and cost), thanks to the slow cell dynamics with respect to the injected perturbations.

References

[1] W. Dai *et al.*, "A review on water balance in the membrane electrode assembly of proton exchange membrane fuel cells," *Int. J. Hydrogen Energy*, vol. 34, no. 23, pp. 9461–9478, 2009.

[2] N. Yousfi-Steiner, P. Moçotéguy, D. Candusso, D. Hissel, A. Hernandez, and A. Aslanides, "A review on PEM voltage degradation associated with water management: Impacts, influent factors and characterization," *J. Power Sour.*, vol. 183, no. 1, pp. 260–274, 2008.

[3] X. Yuan, H. Wang, J. C. Sun, and J. Zhang, "AC impedance technique in PEM fuel cell diagnosis—A review," *Int. J. Hydrogen Energy*, vol. 32, no. 17, pp. 4365–4380, 2007.

[4] J.-M. Le Canut, R. M. Abouatallah, and D. A. Harrington, "Detection of membrane drying, fuel cell flooding, and anode catalyst poisoning on PEMFC stacks by electrochemical impedance spectroscopy," *J. Electrochem. Soc.*, vol. 153, no. 5, pp. A857–A864, 2006.

[5] W. Mérida, D. A. Harrington, J. M. Le Canut, and G. McLean, "Characterisation of proton exchange membrane fuel cell (PEMFC) failures via electrochemical impedance spectroscopy," *J. Power Sour.*, vol. 161, no. 1, pp. 264–274, 2006.

[6] N. Fouquet, C. Doulet, C. Nouillant, G. Dauphin-Tanguy, and B. Ould-Bouamama, "Model based PEM fuel cell state-of-health monitoring via ac impedance measurements," *J. Power Sour.*, vol. 159, no. 2, pp. 905–913, 2006.

[7] T. Kurz, A. Hakenjos, J. Krämer, M. Zedda, and C. Agert, "An impedance-based predictive control strategy for the state-of-health of PEM fuel cell stacks," *J. Power Sour.*, vol. 180, no. 2, pp. 742–747, 2008.

[8] M. F. Mathias and S. A. Grot, "System and method for controlling the humidity level of a fuel cell," U.S. Patent 6 376 111, Apr. 23, 2002.

[9] M. Hinaje, I. Sadli, J.-P. Martin, P. Thounthong, S. Raël, and B. Davat, "Online humidification diagnosis of a PEMFC using a static DC–DC converter," *Int. J. Hydrogen Energy*, vol. 34, no. 6, pp. 2718–2723, 2009.

[10] G. Dotelli, R. Ferrero, P. G. Stampino, S. Latorrata, and S. Toscani, "Diagnosis of PEM fuel cell drying and flooding based on power converter ripple," *IEEE Trans. Instrum. Meas.*, vol. 63, no. 10, pp. 2341–2348, Oct. 2014.

[11] G. Dotelli, R. Ferrero, P. G. Stampino, S. Latorrata, and S. Toscani, "Testing of a diagnostic technique for a single PEM fuel cell based on a DC/DC converter," in *Proc. IEEE AMPS*, Aachen, Germany, Sep. 2014, pp. 1–5.

[12] S. L. Ho and K. W. E. Cheng, "Condition monitoring of rotor faults in induction motors by injection of low frequency signals into the supply," in *Proc. 7th Int. Conf. Power Electron. Variable Speed Drives*, Sorrento, Italy, Sep. 1998, pp. 200–205.

[13] C. Demian, A. Mpanda-Mabwe, H. Henao, and G.-A. Capolino, "Detection of induction machines rotor faults at standstill using signals injection," *IEEE Trans. Ind. Appl.*, vol. 40, no. 6, pp. 1550–1559, Nov./Dec. 2004.

[14] F. Briz, M. W. Degner, A. B. Diez, and J. M. Guerrero, "Online diagnostics in inverter-fed induction machines using high-frequency signal injection," *IEEE Trans. Ind. Appl.*, vol. 40, no. 4, pp. 1153–1161, Jul./Aug. 2004.

[15] R. Ferrero, M. Marracci, M. Prioli, and B. Tellini, "Simplified model for evaluating ripple effects on commercial PEM fuel cell," *Int. J. Hydrogen Energy*, vol. 37, no. 18, pp. 13462–13469, 2012.

[16] W. He, G. Lin, and T. V. Nguyen, "Diagnostic tool to detect electrode flooding in proton-exchange-membrane fuel cells," *AIChE J.*, vol. 49, no. 12, pp. 3221–3228, 2003.

[17] F. Barbir, H. Gorgun, and X. Wang, "Relationship between pressure drop and cell resistance as a diagnostic tool for PEM fuel cells," *J. Power Sour.*, vol. 141, no. 1, pp. 96–101, 2005.

[18] G. Dotelli, R. Ferrero, P. G. Stampino, S. Latorrata, and S. Toscani, "Comparison between electrical and pressure measurements to detect PEM fuel cell flooding," in *Proc. IEEE I2MTC*, Pisa, Italy, May 2015, pp. 1–6.

[19] X. Yu, M. R. Starke, L. M. Tolbert, and B. Ozpineci, "Fuel cell power conditioning for electric power applications: A summary," *IET Electr. Power Appl.*, vol. 1, no. 5, pp. 643–656, Sep. 2007.

[20] M. Y. El-Sharkh, A. Rahman, M. S. Alam, P. C. Byrne, A. A. Sakla, and T. Thomas, "A dynamic model for a stand-alone PEM fuel cell power plant for residential applications," *J. Power Sour.*, vol. 138, nos. 1–2, pp. 199–204, 2004.

[21] A. Benaissa, B. Rabhi, A. Moussi, and D. Aissa, "A linear quadratic regulator control of a stand-alone PEM fuel cell power plant," *Frontiers Energy*, vol. 8, no. 1, pp. 62–72, 2014.

[22] P. Thounthong, S. Raël, and B. Davat, "Energy management of fuel cell/battery/supercapacitor hybrid power source for vehicle applications," *J. Power Sour.*, vol. 193, no. 1, pp. 376–385, 2009.

[23] T. Azib, O. Bethoux, G. Remy, C. Marchand, and E. Berthelot, "An innovative control strategy of a single converter for hybrid fuel cell/supercapacitor power source," *IEEE Trans. Ind. Electron.*, vol. 57, no. 12, pp. 4024–4031, Dec. 2010.

[24] R. S. Gemmen, "Analysis for the effect of inverter ripple current on fuel cell operating condition," *J. Fluids Eng.*, vol. 125, no. 3, pp. 576–585, 2003.

[25] W. Choi, J. W. Howze, and P. Enjeti, "Development of an equivalent circuit model of a fuel cell to evaluate the effects of inverter ripple current," *J. Power Sour.*, vol. 158, no. 2, pp. 1324–1332, 2006.

[26] B. Wahdame *et al.*, "Impact of power converter current ripple on the durability of a fuel cell stack," in *Proc. IEEE ISIE*, Cambridge, U.K., Jun./Jul. 2008, pp. 1495–1500.

[27] R. Ferrero, M. Marracci, and B. Tellini, "Single PEM fuel cell analysis for the evaluation of current ripple effects," *IEEE Trans. Instrum. Meas.*, vol. 62, no. 5, pp. 1058–1064, May 2013.

[28] G. Dotelli, R. Ferrero, P. G. Stampino, and S. Latorrata, "Analysis and compensation of PEM fuel cell instabilities in low-frequency EIS measurements," *IEEE Trans. Instrum. Meas.*, vol. 63, no. 7, pp. 1693–1700, Jul. 2014.